Contributions to Mineralogy and Petrology (2024) 179:44
https://doi.org/10.1007/s00410-024-02125-0

ORIGINAL PAPER

Omphacite breakdown: nucleation and deformation of clinopyroxene-plagioclase symplectites

Sascha Zertani[1] · Luiz F. G. Morales[2,3] · Luca Menegon[1]

Received: 26 December 2023 / Accepted: 18 March 2024

Abstract

The breakdown of omphacite plays an important role in the exhumation and retrogression of eclogites. Additionally, metamorphic reactions associated with grain size reduction have the potential to significantly impact deformation mechanisms and the rheology of crustal rocks. We analyze the breakdown reaction omphacite → diopsidic clinopyroxene + plagioclase ± amphibole and associated microstructures by electron backscatter diffraction. The reaction results in the formation of (diopsidic) clinopyroxene-plagioclase symplectites. Samples were chosen from localities on Holsnøy (western Norway) and Lofoten (northern Norway), that are representative of vermicular symplectites, partly recrystallized symplectites, and deformed symplectites. Interphase misorientation analysis based on the electron backscatter diffraction results reveals that the nucleation of (diopsidic) clinopyroxene-plagioclase symplectites was crystallographically controlled, with the diopside copying the lattice orientation of the omphacite, and the plagioclase growing along diopside planes with favorable, i.e., similar, interplanar spacing. Deformation of the (diopsidic) clinopyroxene-plagioclase symplectites occurred by fracturing, transitioning into grain boundary sliding accommodated by diffusion creep. The results indicate that the formation of vermicular symplectites is not associated with enhanced permeability and fluid flow. Subsequent recrystallisation and grain-size sensitive deformation of the symplectites facilitates fluid redistribution and weakening of the retrogressed eclogites.

Keywords Symplectite · Eclogite · EBSD · Microstructures · Rheology · Fluids

Introduction

Eclogitization of crustal rocks significantly impacts the geodynamic evolution of orogenic systems (Dewey et al. 1993; Godard 2001) and many studies have, thus, focused on the process of eclogitization (e.g., Austrheim 1991; Raimbourg et al. 2007; Engi et al. 2018). Fresh eclogite dominantly consists of omphacite and garnet. However, for eclogites to be exposed at the surface requires their exhumation from great depth, which often results in complete or partial retrogression, and the loss of information about their tectono-metamorphic history up to and at peak metamorphic conditions (e.g., Möller 1998; Labrousse et al. 2004; Yang 2004; McNamara et al. 2012; Zertani et al. 2023).

The first stage of eclogite retrogression is the breakdown of the omphacitic clinopyroxene into symplectites of diopsidic clinopyroxene + plagioclase ± amphibole ± quartz. Omphacite and diopside are both clinopyroxenes, which may lead to confusion. The terminology in this contribution is defined as follows: We refer to clinopyroxene-plagioclase (Cpx-Pl) symplectites when referring to the microstructural association, to establish consistency with previous studies (e.g., Anderson and Moecher 2007), and to diopside when referring to the individual mineral phase within the symplectite. It should be noted that in rare cases the symplectic clinopyroxene may still have an omphacitic composition in particularly Na-rich environments (e.g., O'Brien 1993), but diopsidic clinopyroxene in the symplectites is much more common. In any case, the symplectic clinopyroxene invariably has a lower jadeite content than the primary

Communicated by Dante Canil.

✉ Sascha Zertani
sascha.zertani@mn.uio.no

[1] Njord Centre, Department of Geoscience, University of Oslo, Oslo, Norway

[2] Scientific Center for Optical and Electron Microscopy (ScopeM), ETH Zürich, Zurich, Switzerland

[3] Geological Institute, Department of Earth Sciences, ETH Zürich, Zurich, Switzerland

Published online: 12 April 2024

omphacite (e.g., Boland and van Roermund 1983; O'Brien 1993; Anderson and Moecher 2007).

The reaction was first described by Eskola (1921) and has since been the focus of several studies (Wikström 1970a, 1970b; Mysen 1972; Smyth 1980; Boland and van Roermund 1983; O'Brien 1989; Messiga and Bettini 1990; Joanny et al. 1991; Möller 1998; Yang 2004; Anderson and Moecher 2007; Heidelbach and Terry 2013; Martin and Duchêne 2015; Li et al. 2018; Martin 2019). There is a general consensus that the reaction results from the decompression of eclogites, during which omphacite is destabilized. The reaction is pressure sensitive and it has been shown that it occurs at higher pressure if the jadeite content of the destabilized omphacite is higher (Anderson and Moecher 2007).

Typically, the reaction initially involves the formation of vermicular intergrowths of the reaction products (Mysen 1972), inherently resulting in a substantial grain-size reduction. The grain size itself depends on external factors, dominantly the temperature (Boland and van Roermund 1983), but grain-size variations may also result from two-phase breakdown of omphacite (e.g., O'Brien 1993). It has also been noted, that the reaction is not entirely isochemical and that either the addition of SiO_2 or the oxidation of Fe^{2+} to Fe^{3+} is required for stoichiometric balance (Mysen and Griffin 1973). Likewise, the role of fluids in facilitating the breakdown of omphacite has been discussed, and some studies suggest that at least some amount of fluid is required. For example, Martin and Duchêne (2015) described Cpx-Pl symplectites that formed only in eclogites that contain hydrous phases (phengite), while dry eclogite from the same locality showed no signs of symplectite formation. They conclude that the presence of internal fluids is necessary for the reaction to occur. Similarly, O'Brien (1993) described Cpx-Pl symplectites along omphacite grain boundaries, but the reaction around quartz inclusions in the same samples only occurred if the inclusion was connected to the matrix, e.g., by fractures, suggesting that the reaction only proceeded in the presence of a grain boundary fluid.

In itself, the reaction may substantially impact the bulk rock rheology, and subsequently play a role in the tectonic evolution of mountain belts. For example, some studies have suggested that the breakdown of omphacite can lead to, or assist the rapid exhumation of deeply buried rocks (Dey et al. 2022) and in extreme cases even represent a precursor to partial melting (Feng et al. 2020). Furthermore, similar breakdown reactions that lead to extreme grain-size reductions through the formation of symplectic intergrowths have been shown to facilitate rock weakening, and thus promote deformation and strain localization (e.g., formation of myrmekite; Ceccato et al. 2018).

Although Cpx-Pl symplectites occur in most eclogite localities, their nucleation and deformation behavior are still poorly understood. The study of misorientations along low- and high angle grain boundaries is frequently used to study deformation processes in geological materials (e.g., Lloyd et al. 1997; Neumann 2000; Wheeler et al. 2001). On the other hand, misorientations along phase boundaries (interphase misorientations in the following; Morales 2022) are less commonly studied although special orientation relationships may provide information on phase transformation processes that lead to 'special orientations'; i.e., systematically coincident lattice planes and/or axes (McNamara et al. 2012; Morales et al. 2018). Such orientation relationships may be useful for constraining nucleation processes and subsequent deformation mechanisms of the reaction products.

In this contribution we analyze several Cpx-Pl symplectites with electron backscatter diffraction (EBSD). Samples were collected from two localities; (i) the island of Holsnøy (Lindås nappe, western Norway) and (ii) Lofoten (northern Norway). We determine crystallographic relationships between the omphacite and the reaction products, as well as between the reaction products themselves during nucleation. We investigate how these relationships are modified during recrystallization and deformation, and identify the mechanisms involved. The results are discussed in the context of the impact of Cpx-Pl symplectites on rheology and fluid flow during eclogite retrogression.

Geological context

Holsnøy, Lindås nappe, western Norway

The island Holsnøy (Lindås nappe) exposes granulite-facies, lower-crustal, basement rocks of the hyperextended, pre-Caledonian margin of the Baltica-affiliated Jotun microcontinent (Jakob et al. 2019). These rocks are cross-cut by an eclogite shear zone network (Austrheim 1987). Eclogites occur in centimeter to hundreds-of-meters thick shear zones (e.g., Raimbourg et al. 2005; Zertani et al. 2019; Bras et al. 2021; Kaatz et al. 2021) and as statically eclogitized zones (e.g., Jamtveit et al. 2000; Putnis et al. 2021; Zertani et al. 2022; Baïsset et al. 2023). Fluid-induced eclogitization occurred at 423–430 Ma (Glodny et al. 2008; Jamtveit et al. 2021) at 650–750 °C and 1.7–2.1 GPa (e.g., Jamtveit et al. 1990; Bhowany et al. 2018; Zhong et al. 2019). The Lindås nappe eclogites have been partially overprinted at amphibolite-facies conditions (e.g., Centrella 2019; Moore et al. 2020).

Lofoten, northern Norway

The Lofoten archipelago (northern Norway) exposes the lower continental crust of Baltica. The lithologies are dominantly Paleoproterozoic gneisses that have been intruded by a suite of AMCG (anorthosite, mangerite, charnockite, granite) rocks between 1.9 and 1.7 Ga, at lower-crustal,

granulite-facies conditions (Markl et al. 1998; Corfu 2004). Eclogite-facies metamorphism is evidenced by strongly retrogressed eclogite-facies shear zones (Steltenpohl et al. 2003; 2011; Fournier et al. 2014; Zertani et al. 2023). The relation of these shear zones with the Caledonian orogenic cycle is a matter of debate but recent geochronological results suggest that eclogitization likely occurred during the Caledonian collision at ~ 428 Ma (Jaranowski et al. 2023).

Eclogite-facies rocks in the area have been strongly to completely retrogressed at amphibolite-facies conditions. For this reason, determination of the pressure–temperature (P–T) conditions during the eclogite-facies event is difficult (see discussion in Zertani et al. 2023). Estimates range from 1.1 to 2.8 GPa at 650–780 °C (Markl and Bucher 1997; Froitzheim et al. 2016).

Sample context and microstructural description

SZ-N-018

SZ-N-018 is a massive to weakly-foliated eclogite (Online resources 1, Fig. S1) that was collected from the northwestern tip of Holsnøy (locations for all samples provided in Online resources 1, Table S1). The rock consists mainly of garnet, omphacite, amphibole, and clinozoisite (Fig. 1a). The eclogitic foliation dips moderately to the east (074/44; dip azimuth/dip) and is formed by the weak shape preferred orientation (SPO) of omphacite. Cpx-Pl symplectites are abundant along omphacite grain boundaries and are typically 10–100 µm wide (Fig. 1a, b). In addition to clinopyroxene and plagioclase, the symplectites contain significant amounts of amphibole, that is either small and integrated into the dominantly vermicular microstructure, or occurs as larger (~ 30 µm) grains.

L-042

L-042 was collected from the Ramberg locality in Lofoten, northern Norway, that represents one of the main eclogite localities in the area (e.g., Froitzheim et al. 2016). The structural context of these rocks has been described in detail by Zertani et al. (2023). The area exposes a few-hundred-meters wide, amphibolite shear zone, that preserves microscopic evidence of prior eclogitization. This shear zone anastomosed around meter to tens-of-meters-sized low strain domains. The sample was collected from one of these low-strain blocks (Online resources 1, Fig. S1). It preserves some omphacite in the matrix. However, most of the rock consists of Cpx-Pl symplectites and garnet (Fig. 1c). The Cpx-Pl symplectites have both vermicular and granular portions.

WP039A

WP039A is a strongly-foliated amphibolite (Online resources 1, Fig. S1) that was collected from the same locality as L-042, but represents the main shear zone fabric. It dominantly consists of fine-grained amphibole and plagioclase anastomosing around large garnet porphyroclasts (Fig. 1d). Prior eclogitization is evidenced by omphacite inclusions in garnet and by Cpx-Pl symplectites in the matrix (Fig. 1d–f). These are typically vermicular in their core, and have a granular rim. Cpx-Pl symplectites range from isometric to sigmoidal or strongly elongated parallel to the amphibolite-foliation (Fig. 1d, f). Amphibole within the Cpx-Pl symplectites is only present as a few isolated grains within the granular parts, however, the Cpx-Pl symplectite is typically rimmed entirely by amphibole (Fig. 1e, f).

Methods

Backscattered electron (BSE) images were collected using a Hitachi SU5000 FE scanning electron microscope and a Hitachi TM4000 Plus Tabletop scanning electron microscope, both located at the Department of Geosciences, University of Oslo. The following operating conditions were used; 15 kV acceleration voltage and 11–12 mm working distance.

The Hitachi SU5000 FE scanning electron microscope was additionally used for EBSD analysis. Operating conditions were 20 kV acceleration voltage, 22 mm working distance, 30–35 ms exposure time, 0.4–0.5 µm step size, and 70° sample tilt. EBSD pattern indexing was performed with the Esprit software (v. 2.3; Bruker). Postprocessing of EBSD data was performed using the MTEX toolbox v. 5.10.0 (Hielscher and Schaeben 2008). The data are presented as phase maps, inverse pole figure (IPF) maps, misorientation to mean orientation (Mis2Mean) maps, pole figures, and misorientation angle histograms. Colormaps in Mis2Mean maps and pole figures are from Crameri (2018).

Interphase misorientation analysis was conducted using the procedure described in Morales (2022). To test the influence of the cell parameters of the phases used during indexing of the EBSD maps every map was indexed twice; once using andesine (cell parameters: $\alpha = 93.44°$, $\beta = 116.21°$, $\gamma = 90.23°$, $a = 8.2$ Å, $b = 13.0$ Å, $c = 7.1$ Å) and once using oligoclase (cell parameters: $\alpha = 94.06°$, $\beta = 116.5°$, $\gamma = 88.59°$, $a = 8.2$ Å, $b = 13.0$ Å, $c = 7.1$ Å), both from the Esprit (Bruker) database. Indexing rates between the two versions varied slightly (from andesine to oligoclase by 0.2–1.1 percentage points, see Online resource 1, Table S2) with the oligoclase consistently resulting in higher indexing rates. This is consistent with the available mineral chemical data that show that the dominant plagioclase composition

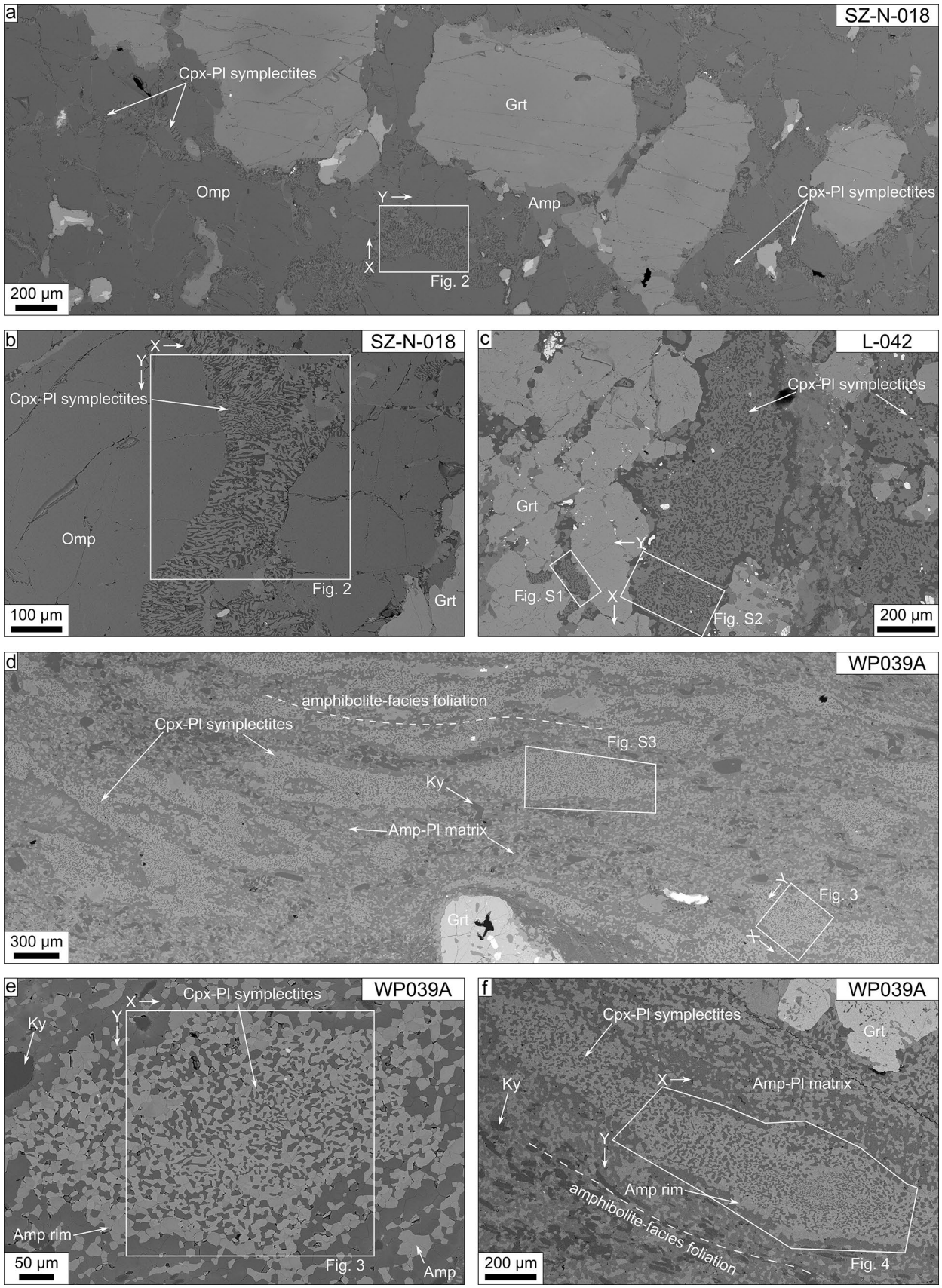
a
SZ-N-018
Cpx-Pl symplectites
Grt
Omp
Amp
Cpx-Pl symplectites
Y
X
Fig. 2
200 µm
b
SZ-N-018
X
Y
Cpx-Pl symplectites
Omp
Fig. 2
Grt
100 µm
c
L-042
Cpx-Pl symplectites
Grt
Y
Fig. S1
X
Fig. S2
200 µm
d
WP039A
amphibolite-facies foliation
Cpx-Pl symplectites
Fig. S3
Ky
Amp-Pl matrix
Y
Fig. 3
X
Grt
300 µm
e
WP039A
Cpx-Pl symplectites
X
Y
Ky
Amp rim
Fig. 3
Amp
50 µm
f
WP039A
Cpx-Pl symplectites
Grt
Ky
X
Amp-Pl matrix
Y
Amp rim
amphibolite-facies foliation
Fig. 4
200 µm

◂**Fig. 1** Backscattered electron (BSE) images of the studied Cpx-Pl symplectites. White outlines in all images show the area mapped by EBSD and the sample reference frame used in subsequent figures is given as X and Y, with the arrow showing the positive direction. **a** BSE image of SZ-N018-1 showing garnet (Grt), amphibole (Amp), omphacite (Omp), and Cpx-Pl symplectites along omphacite grain boundaries. **b** Zoomed-in area from **a**. The white box in **a** and **b** show the same area, but the image in **b** is rotated by 90° with respect to the image in **a** to show the vermicular Cpx-Pl symplectites along omphacite grain boundaries. **c** Microstructure of the retrogressed eclogite (L-042) showing Cpx-Pl symplectites (L-042-1, left; L-042-2, right) adjacent to a garnet cluster. The sample reference frame (X, Y) is the same for both white boxes. **d** Overview BSE image of the main fabric of WP039A showing abundant Cpx-Pl symplectites (WP039A-1, bottom right; WP039A-2, center) elongated parallel to the main foliation (dashed line). The sample reference frame (X, Y) is the same for both white boxes. **e** Zoomed-in image to the area of the white box in the lower right corner of **d**, showing a relatively isometric Cpx-Pl symplectite (WP039A-1) with a vermicular core but dominantly granular microstructure. **f** BSE image of a strongly elongated Cpx-Pl symplectite (WP039A-3) with a vermicular core and granular tails. The figures that show the EBSD results of each area are provided in the panels. Those not shown in the main manuscript are provided in Online resource 1, Figs. S2–S4

plots in the oligoclase field (Online resource 1, Fig. S5). Throughout this contribution we thus use the maps indexed with oligoclase. A comparison of the effect of variations in cell parameters is shown in Online resource 1, Fig. S6. For diopside a model with the cell parameters $\beta = 106.02°$, $a = 9.7$ Å, $b = 8.9$ Å, and $c = 5.3$ Å was used for all maps except for site SZ-N-018-1.

SZ-N-018-1 contains both the preserved omphacite and the symplectic clinopyroxene, resulting in difficulties during indexing, due to the very similar cell parameters. We thus indexed this map four times in the combinations andesine-diopside, andesine-omphacite, oligoclase-diopside, and oligoclase-omphacite. The maps were then merged in MTEX so that the parent grains used the omphacite indexing and the symplectic grains used the diopside indexing resulting in the final combinations of diopside-omphacite-andesine and diopside-omphacite-oligoclase. Cell parameters were $\beta = 106.78°$, $a = 9.7$ Å, $b = 8.8$ Å, and $c = 5.3$ Å for diopside, and $\beta = 106.8°$, $a = 9.6$ Å, $b = 8.8$ Å, and $c = 5.3$ Å for omphacite. The four individual maps are shown in Online resource 1, Fig. S7. Cell parameters of all models used are given in Online Resource 1, Table S3. During postprocessing the following steps were used: (1) grain construction using 10° misorientation as a threshold; (2) grains smaller than 5 pixels were removed; (3) non-indexed regions smaller than 5 pixels were filled; (4) grain construction was repeated.

Results

In the following the studied symplectites will be labelled by sample name and site number. In SZ-N-018 one symplectite was analyzed (SZ-N-018-1), in L-042 two symplectites were analyzed (L-042-1, L-042-2), and in WP039A three symplectites were analyzed (WP039A-1, WP039A-2, WP039A-3). Additionally, with each mention the dominant type of microstructure (vermicular or granular) is provided in parentheses. Note that most analyzed symplectites contain vermicular and granular parts, and the label only refers to the dominant microstructure.

EBSD analysis

Diopside

Diopside occurs as vermicular intergrowths with plagioclase or is granular (Fig. 1), and is present exclusively within the Cpx-Pl symplectites throughout all samples. Inverse pole figure (Z-direction, IPFZ) maps show that vermicular portions are large, irregularly shaped, coherent grains (Fig. 2). In granular portions grains are smaller, trend toward isometric in shape, and orientations are dispersed (Figs. 3, 4). Internal misorientations can be up to ~ 16° and are strongest in the vermicular portion of Cpx-Pl symplectites (Figs. 2, 4), while granular portions show little or no internal misorientations (Figs. 3, 4). Pole figures yield strong crystallographic preferred orientations (CPO) of (100), (010), and (001)-poles, with CPO strength being at least 5.2 multiples of uniform distribution (m.u.d.) and up to 21.7 m.u.d. (Fig. 2e). CPO strength is generally lower in Cpx-Pl symplectites with a higher amount of granular diopside, but even in those Cpx-Pl symplectites the CPO strength in the vermicular core is significantly higher than that of the granular portion (Fig. 4e, f).

Plagioclase

Plagioclase within the Cpx-Pl symplectites is vermicular or granular, and associated with diopside. Additionally, plagioclase occurs in the matrix of WP039A together with amphibole (Fig. 1). Textural features of plagioclase in the Cpx-Pl symplectites are similar to those of diopside: patches of vermicular plagioclase have the same crystallographic orientation with respect to the sample reference frame (Fig. 5a), while the orientation of granular plagioclase is more dispersed (Fig. 5b), and internal misorientations (up to 15°) are typically larger in vermicular portions compared to granular ones (Fig. 5c). Likewise, plagioclase

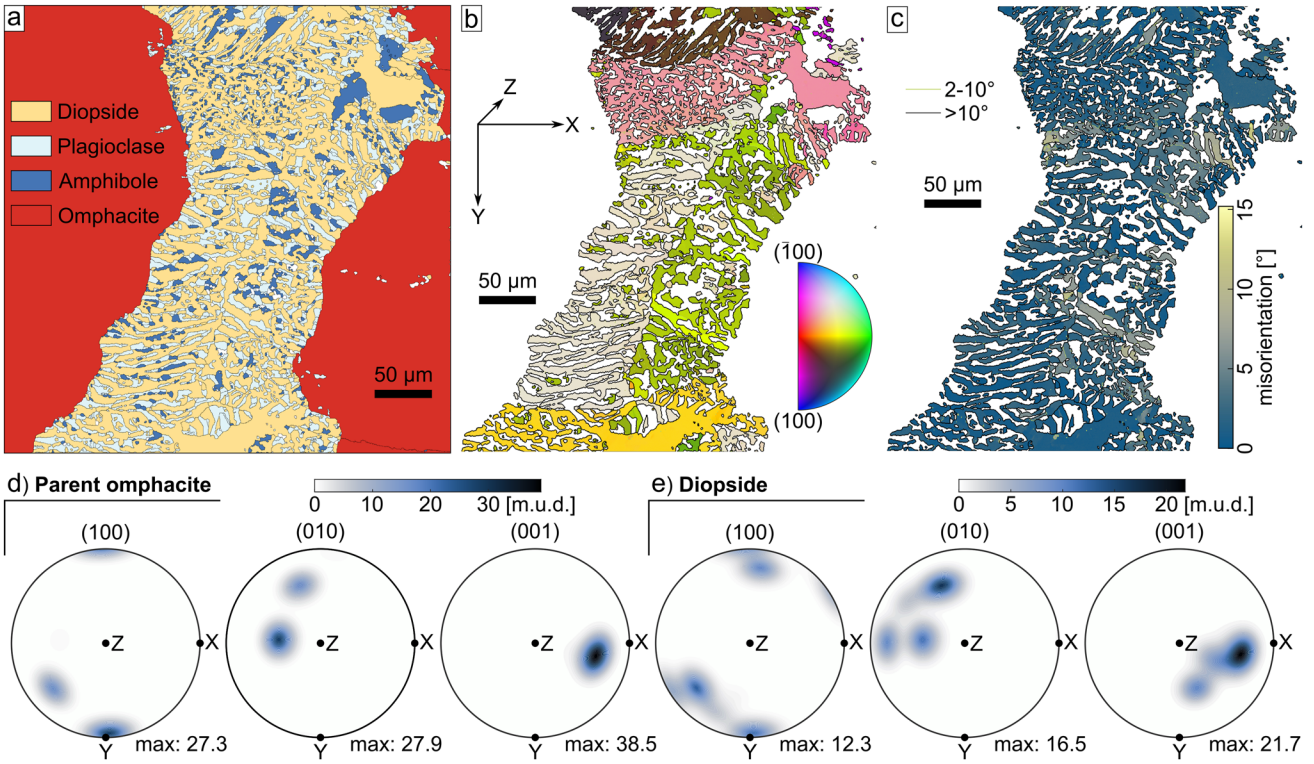

Fig. 2 Results of EBSD analysis of vermicular diopside and parent omphacite (SZ-N-018-1). **a** Phase map; **b** Inverse pole figure (Z-direction; IPFZ) map of vermicular diopside. The sample reference frame is given in the upper left corner. **c** Misorientation to mean orientation (Mis2Mean) map. **d** Pole figures showing the distribution of poles to crystallographic planes in the parent omphacite (red in **a**). **e** Pole figures showing the distribution of poles to crystallographic planes of vermicular diopside (yellow in **a**). Maxima given at the bottom of each pole figure are in multiples of a uniform distribution (m.u.d.)

displays strong CPO in pole figures with up to 16.0 m.u.d. CPO is most clearly developed in (100) and/or (010)-poles but also evident in (001)-poles (Fig. 5d). As for diopside, plagioclase CPO strength is lower in granular portions of the Cpx-Pl symplectites (Fig. 5e).

Interphase misorientation analysis

In the following we examine orientation relationships between diopside and plagioclase derived from the EBSD results distinguishing between (i) uniform distribution, i.e., the distribution if grains are randomly oriented, (ii) uncorrelated misorientation angles, i.e., between randomly selected grain pairs, and (iii) correlated misorientation angles, i.e., between neighboring pairs. The misorientation angle distribution between plagioclase and diopside expected for a uniform distribution (uniform misorientation angle distribution) is defined by a gradual, non-linear increase in frequency from 0° to 90° followed by a gradual non-linear decrease to 180° (purple line in Fig. 6). Uncorrelated misorientation angle distributions (red lines in Fig. 6) in general follow the trend of the uniform distribution with some marked differences. In SZ-N-018-1 and L-042-1 (vermicular) misorientation angles in the range 85–155° and 77–130°, respectively, are significantly more frequent, while lower misorientation angles are less frequent than the uniform distribution (Fig. 6a, b). For L-042-2 (vermicular) and WP039A-2 (granular) misorientation angles are less frequent in the range 77–127° and 78–137° (Fig. 6c, e), respectively, and for WP039A-2 (granular) lower angle misorientations are more frequent (Fig. 6d). For WP039A-1 and 3 (granular), however, the uncorrelated misorientation angle distribution follows the uniform distribution with only minor deviations (Fig. 6d, f).

Similarly, correlated misorientation angle distributions deviate strongly from the uniform distribution in most of the Cpx-Pl symplectites studied here (Fig. 6). Most pronounced is a higher frequency of misorientation angles in SZ-N-018-1 (vermicular) in the range 77–103° (Fig. 6a), and in L-042-1 (vermicular) in the range 73–113° (Fig. 6b). Higher frequency of misorientation angles is also evident in the range 140–170°, 135–160°, and 124–164° for SZ-N-018-1 (vermicular), L-042-2 (vermicular), and WP039A-2 (granular), respectively (Fig. 6a, c, e). In the same Cpx-Pl symplectites, significantly less

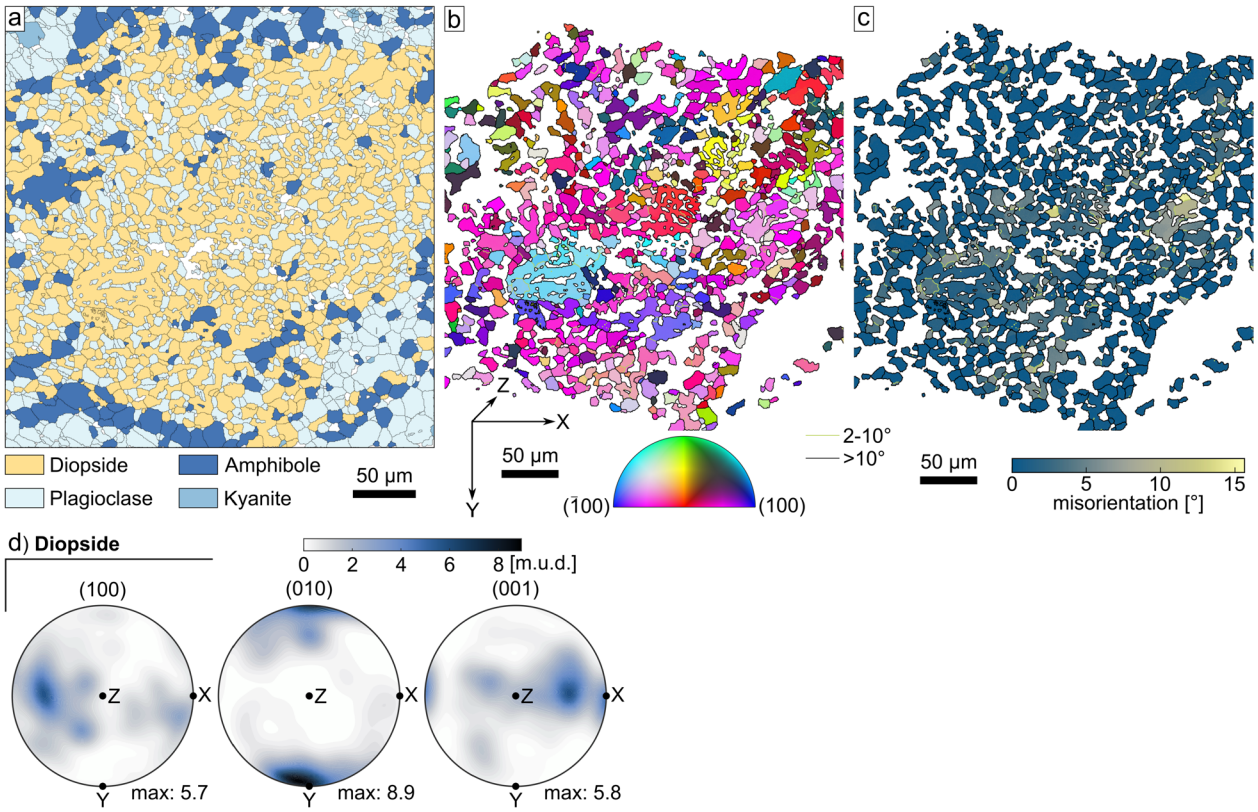

Fig. 3 Results of EBSD analysis of diopside in a dominantly granular Cpx-Pl symplectite (WP039A-1). **a** Phase map; **b** IPFZ map of diopside. The sample reference frame is given in the lower left corner. **c** Mis2Mean map of diopside. **d** Pole figures showing the distribution of poles to crystallographic planes in diopside. Maxima given at the bottom of each pole figure are in multiples of a uniform distribution (m.u.d.)

frequent misorientation angles are observed in the range 104–140°, 87–114°, and 67–123° in SZ-N-018-1 (vermicular), L-042-2 (vermicular), and WP039A-2 (granular), respectively (Fig. 6a, c, e). Additionally, there are significantly lower frequencies observed at low misorientation angles in SZ-N-018-1 and L-042-1 (vermicular; Fig. 6a, b). Misorientation angles in WP039A-1 and WP039A-3 (granular) most closely follow the uniform distribution, though some deviations exist (Fig. 6d, f).

The uniform misorientation axis distribution indicates a weak maximum (2 m.u.d.) parallel to (h0l) planes both with respect to the diopside and plagioclase reference frames (Fig. 7a). Contrarily, the orientation plots of the misorientation axes yield strong preferred orientations (Fig. 7). Particularly Cpx-Pl symplectites in SZ-N-018-1 and L-042-1 (vermicular) yield strong preferred orientations of ~ 20 and ~ 32 m.u.d., respectively. The weakest preferred alignment of misorientation axes is found in WP039A-1 and WP039A-2 (granular) with 7.6 and 5.7 m.u.d., respectively.

The crystallographic axes and poles that correlate to the maxima in correlated misorientation axis distributions are shown in Fig. 7 for all samples over the entire range of angles. Qualitatively, results from Cpx-Pl symplectites with a stronger preferred alignment of misorientation axes yield point maxima, while those with weaker alignment may have a weak girdle distribution (Fig. 7g), reminiscent of the uniform distribution (Fig. 7a).

Discussion

Nucleation of Cpx-Pl symplectites

The breakdown of omphacite to Cpx-Pl symplectites is typically attributed to decompression and can occur along omphacite grain boundaries or in the interior of omphacite grains (e.g., Anderson and Moecher 2007). From our three samples only one (SZ-N-018, vermicular) preserves a clear relationship of Cpx-Pl symplectite formation along grain boundaries (Fig. 1a, b). The Cpx-Pl symplectite

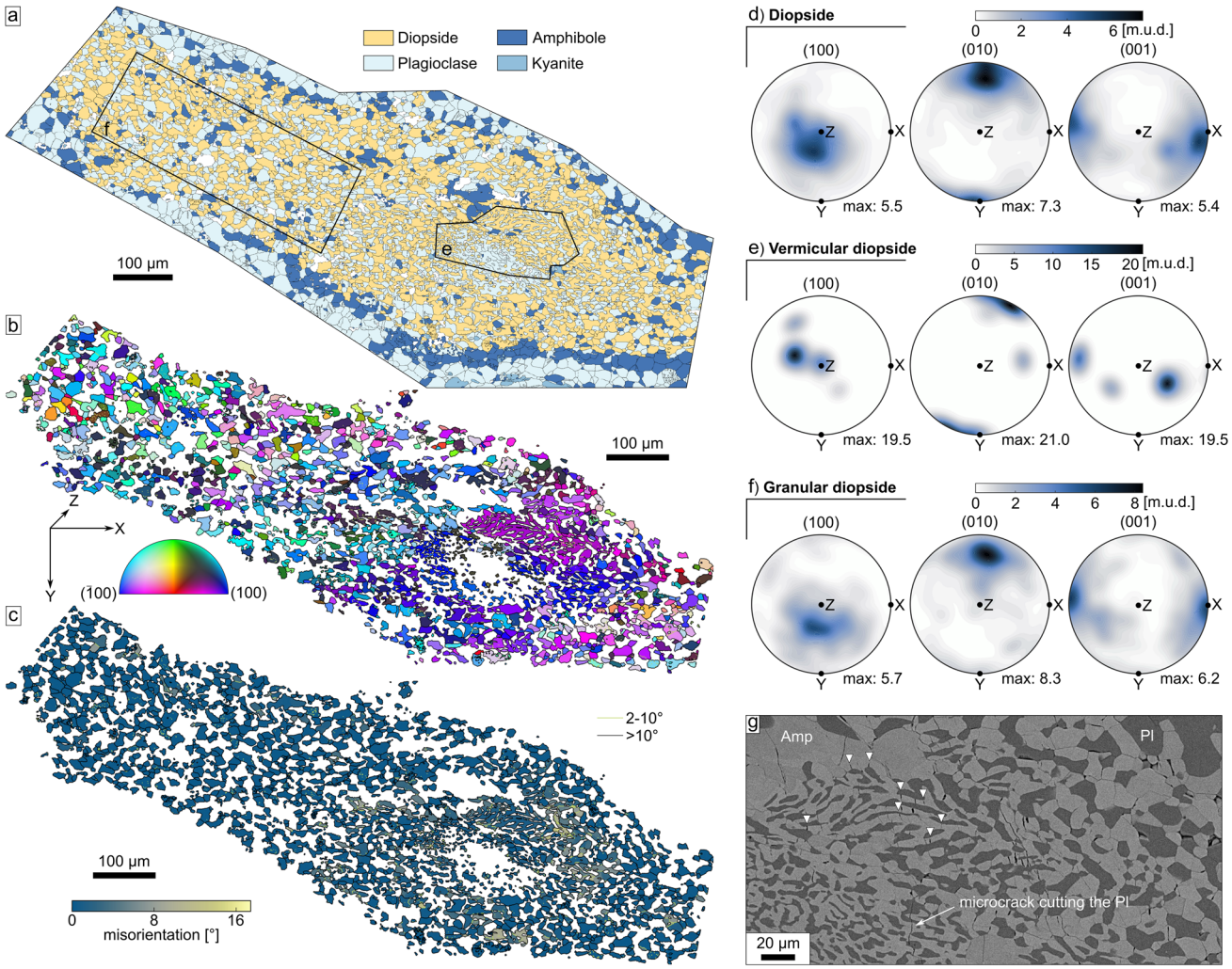

Fig. 4 Results of EBSD analysis of diopside in a recrystallized Cpx-Pl symplectite (WP039A-3) that has been deformed. **a** Phase map; **b** IPFZ map of diopside. The sample reference frame is given in the lower left corner. **c** Mis2Mean map of diopside. **d** Pole figures showing the distribution of poles to crystallographic planes in diopside. **e** Pole figures showing the distribution of diopside in the vermicular portion (area shown in **a**). **f** Pole figures showing the distribution of diopside in the granular portion of the symplectite (area shown in **a**). Maxima given at the bottom of each pole figure are in multiples of a uniform distribution (m.u.d.). **g** BSE image of the vermicular part of the symplectite (approximately **e** in **a**). White triangles show microcracks in diopside. *Amp* amphibole, *Pl* plagioclase

microstructure is entirely vermicular, and the adjacent omphacite grains show no signs of deformation, consistent with the reaction occurring statically.

The diopside orientation is controlled by the crystallographic orientation of the 'parent' omphacite (Fig. 2d, e), in that it either has the orientation of the grain that is being replaced, or the orientation of the adjacent omphacite (Online resource 1, Fig. S7). Components of both orientations are preserved in the symplectite and by 'parent' we thus refer to the grain being replaced or the adjacent grain. Based on optical investigation it has been shown that the symplectic diopside grows in several 'lobes' that are consistent in orientation with the adjacent omphacite (O'Brien, 1989; 1993), consistent with the results presented here (see also Online resource 1, Fig. S7). Based on X-ray precession photographs in kimberlitic omphacites, Smyth (1980) found that lamellae of newly formed clinopyroxene within the host grain share the same c-axis, while a- and b-axes differ strongly. In contrast, the example presented here indicates that the diopside perfectly mimics the omphacite orientation, i.e., the replacement of omphacite by diopside is topotactic.

Interestingly, this topotactic replacement leads to the formation of an interconnected skeleton of diopside with consistent orientation. The general characterization of Cpx-Pl symplectites as fine-grained reaction products does thus not hold for the diopside. In fact, the diopside grain size is significantly larger than the grain size of plagioclase at

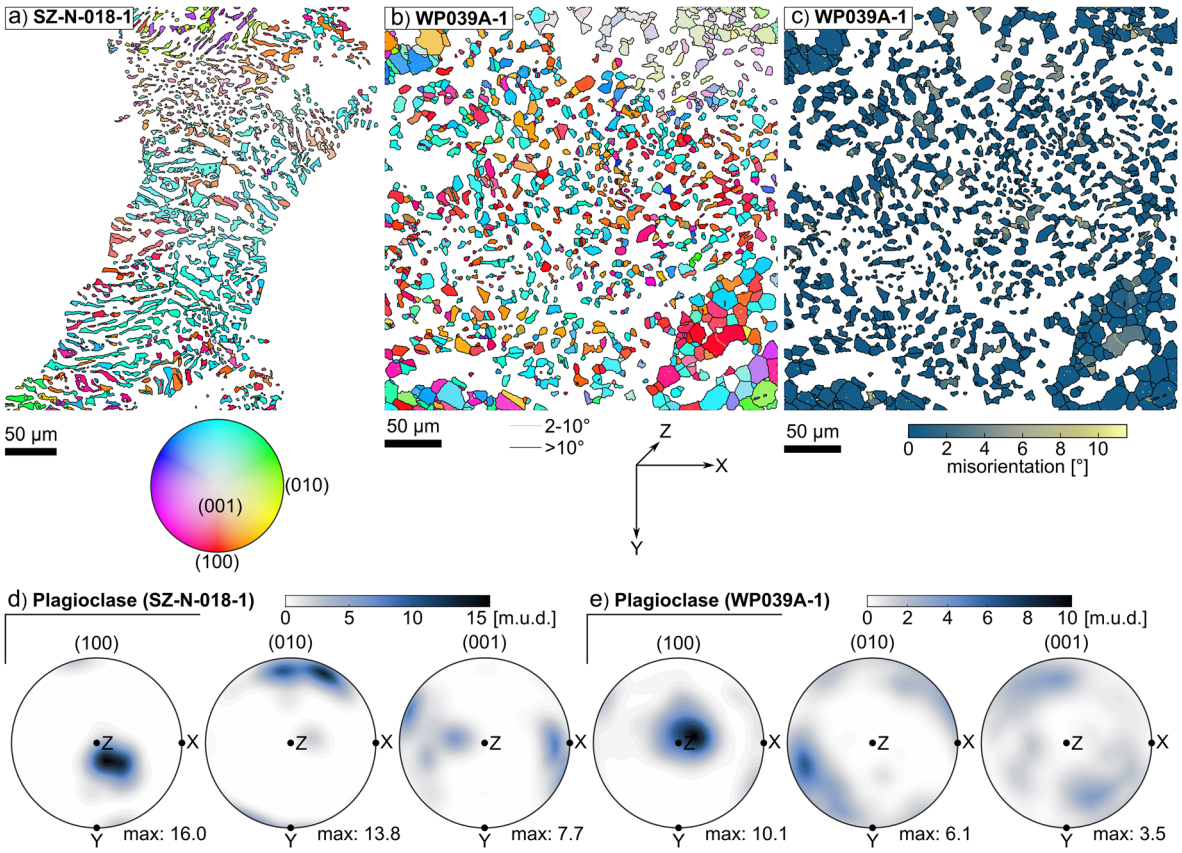

Fig. 5 Results from EBSD analysis of plagioclase. **a** IPFZ map of plagioclase in SZ-N-018-1 (vermicular; Fig. 2). **b** IPFZ map of plagioclase in WP039A-1 (granular; Fig. 3). **c** Mis2mean map of plagioclase in WP039A-1 (granular). **d** Pole figures of plagioclase in SZ-N-018-1 (vermicular). **e** Pole figures of plagioclase in WP039A-1 (granular)

least if the reaction occurs statically (Fig. 2a, b). While only one of our examples preserves the 'parent' omphacite, also the other Cpx-Pl symplectites preserve a dominantly strong CPO and a large (> 40 µm) grain size of diopside in their vermicular core. In WP039A-3 (granular), for example, diopside CPO is comparatively moderate with up to 7.3 m.u.d.. However, in the same example and considering only the vermicular part of the Cpx-Pl symplectite, diopside CPO is significantly stronger (21.0 m.u.d.; Fig. 4d–f). These results are consistent with a study by Heidelbach and Terry (2013), where symplectic diopside is also characterized by a strong CPO. Additionally, topotactic relationships during symplectite forming reactions are not limited to the Cpx-Pl symplectites studied here. For example, the replacement of K-feldspar by plagioclase during myrmekite formation is topotactic (Ceccato et al. 2018), as is the replacement of KBr crystals during hydrothermal experiments (Spruzeniece et al. 2017).

Our EBSD analyses further show that diopside—particularly when vermicular—is characterized by internal misorientations of up to ~ 16° (Figs. 2, 3, 4). Spruzeniece et al. (2017) proposed that misorientations within symplectic intergrowths may mimic distortions of the crystal lattice of the 'parent' grain that were transferred to the reaction product. Information about lattice distortions and low-angle boundaries may thus be preserved in the reaction products. For SZ-N-018-1 (vermicular) the preserved omphacite does not yield significant internal misorientations (Online resource 1, Fig. S8). It thus seems unlikely that the misorientations observed in the symplectic diopside are inherited from the parent grain. Lattice distortions are rather diffuse, and only few sharp low-angle boundaries have formed (Fig. 2c), rendering a statistical approach to their interpretation difficult. The breakdown of omphacite to Cpx-Pl symplectites results in a volume increase (densities: plagioclase = 2.7 g/cm^3; diopside = 3.2 g/cm^3; omphacite = 3.5 g/cm^3; Deer et al. 2013). The simplest explanation is thus that the observed lattice distortions are reaction induced, and act to accommodate the volume increase by bending of the crystal lattice.

Plagioclase in the vermicular parts of symplectites occurs as fine grains surrounded by diopside. The CPO of plagioclase is also strong with up to ~ 16 m.u.d., particularly of

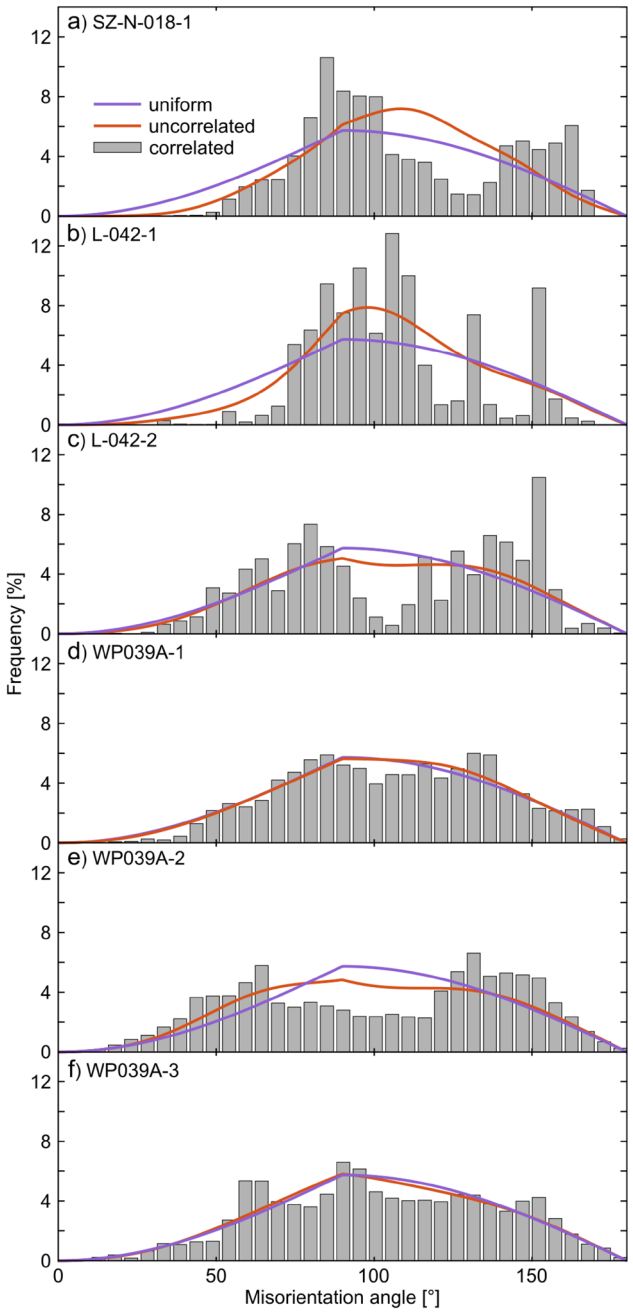

Fig. 6 Interphase misorientation angles between diopside and plagioclase for the symplectites **a** SZ-N-018-1 (vermicular), **b** L-042-1 (vermicular), **c** L-042-2 (vermicular), **d** WP039A-1 (granular), **e** WP039A-2 (granular), and **f** WP039A-3 (granular). Shown are the uniform distribution (purple), the uncorrelated distribution (orange) and the histogram of correlated misorientation angles

(100), suggesting that plagioclase nucleation is also crystallographically controlled by the host omphacite. This result is in contrast to the results of Heidelbach and Terry (2013), that found only weak CPO of plagioclase in Cpx-Pl symplectites. Similar to diopside, internal misorientations of plagioclase are stronger in the vermicular parts, and likely caused by the same effect: lattice distortion due to volume increase.

As is expected, given the strong CPO of plagioclase and diopside, the uncorrelated misorientation angle distribution deviates significantly from the uniform distribution, particularly for the symplectites with a dominantly vermicular microstructure (Fig. 6a–c). Even stronger deviation is observed for correlated misorientation angles, suggesting the presence of a 'special orientation relationship' (in the sense of Morales 2022) between plagioclase and diopside. Indeed, plots of misorientation axis distributions yield strong point maxima (up to 32 m.u.d.) for dominantly vermicular Cpx-Pl symplectites (Fig. 7b–d), that stand in stark contrast to the theoretical uniform distribution (Fig. 7a), which predicts a weak girdle along (h0l). Considering the correlated misorientation angle distribution (Fig. 6) of the dominantly vermicular Cpx-Pl symplectites SZ-N-018-1 (vermicular; Fig. 6a), L-042-1, and L-042-2 (vermicular; Fig. 6b, c), frequencies higher than the uniform distribution are present in the ranges ~ 75–110° and ~ 140–165°. Individual analysis of these ranges yields several orientation relationships, that are listed in Table 1 (Fig. 8). We further calculated the interplanar spacing (d) for these planes using the equations given in Appendix 3 of Kelly and Knowles (2012):

$$\frac{1}{d^2} = h^2a^{*2} + k^2b^{*2} + dl^2c^{*2} + 2klb^*c^*\cos\alpha^* + 2lhc^*a^*\cos\beta^* + 2hka^*b^*\cos\gamma^*$$

where h, k, and l are the Miller indices of the crystallographic plane, and

$$a^* = \frac{bc\sin\alpha}{V}, b^* = \frac{ca\sin\beta}{V}, c^* = \frac{ab\sin\gamma}{V}.$$

The cell parameters of the mineral in question are given as a, b, c, α, β, and γ, and

$$V = abc\sqrt{1 - \cos^2\alpha - \cos^2\beta - \cos^2\gamma + 2\cos\alpha\cos\beta\cos\gamma}$$

The results yield ratios between $d_{Plagioclase}$ and $d_{Diopside}$ of ~ 1 (Table 1), suggesting that the strong orientation relationship is controlled by the favorable distance between lattice planes of diopside and plagioclase.

Recrystallization and deformation of Cpx-Pl symplectites

Several of the Cpx-Pl symplectites presented here, particularly those from sample WP039A (granular), provide insight into how the microstructure and crystallographic relationships of Cpx-Pl symplectites are modified during recrystallization and deformation. Anderson and Moecher (2007) suggested that recrystallization and coarsening of grains within the Cpx-Pl symplectites provides evidence of

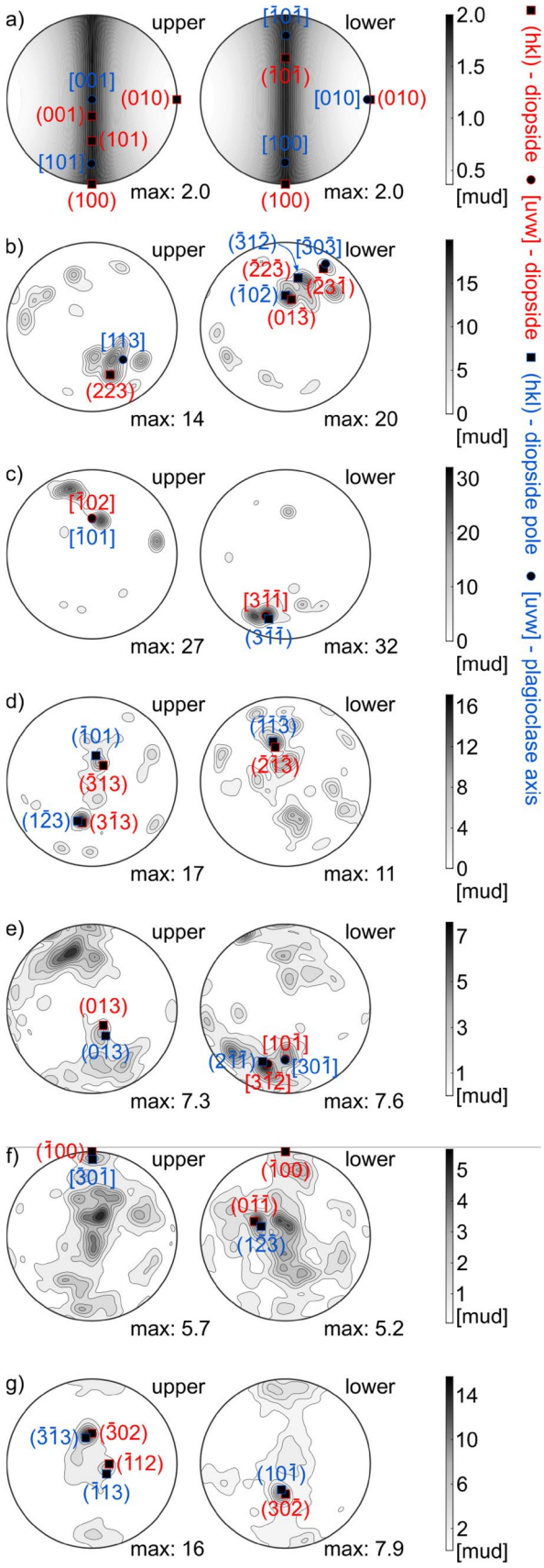

Fig. 7 Misorientation axis distributions for diopside-plagioclase pairs. **a** Theoretical uniform misorientation axis distribution, showing the diopside reference frame as poles to planes (in red) and the plagioclase reference frame as crystallographic axes (in blue). **b**–**g** Correlated misorientation axis distribution for all samples: **b** SZ-N-018-1 (vermicular), **c** L-042-1 (vermicular), **d** L-042-2 (vermicular), **e** WP039A-1 (granular), **f** WP039A-2 (granular), **g** WP039A-3 (granular). Poles and axes labelled in each diagram correspond to the maxima in the respective plots

low geothermal gradients during exhumation, and subsequently that the rocks were exposed to high temperatures for relatively long times. The crystallographic data presented here, however, indicates that the initially formed diopside represents an interconnected ('skeletal') framework for the nucleation of plagioclase within (Fig. 2). The diopside grain size must thus initially be reduced during recrystallization, rather than coarsened.

Examination of the vermicular portions of otherwise strongly recrystallized Cpx-Pl symplectites reveals two types of microcracks. The first is characterized by relatively long cracks that cut through several diopside lamellae and also through the plagioclase. The second are regularly-spaced microcracks in diopside, perpendicular to the length of the lamellae (Fig. 4g), that occur only in the vermicular part of the Cpx-Pl symplectites, and do not cut through the adjacent plagioclase. Frequently, they also do not cut the entire lamellae. This second type of micocracks may be coeval with deformation of the symplectites at amphibolite-facies conditions. The lack of such fractures in the granular diopside may also indicate that the aspect ratio of the diopside lamellae plays a role in facilitating fracturing. The most probable mechanism for the grain size reduction of diopside is thus fracturing, consistent with experimental studies at pressure–temperature conditions comparable to those of eclogite retrogression and deformation in Holsnøy and Lofoten (e.g., Marti et al. 2018), which have been estimated to be 0.8–1.0 GPa and 600 °C (Glodny et al. 2008) and 0.7–1.1 GPa and 650–700 °C (Zertani et al. 2023), respectively.

The grain size reduction of diopside is significant and such drastic grain size reduction may lead to the activation of grain size sensitive deformation mechanisms. Marti et al. (2018) deformed plagioclase-diopside mixtures experimentally at 800 °C and 1.0 and 1.5 GPa. They found that the substantial reduction in grain size leads to the activation of dissolution–precipitation creep accommodated by grain boundary sliding. The most striking feature observed from our EBSD analysis is that deformation of the Cpx-Pl symplectites is accompanied by a reduction in CPO strength, accompanied by the development of a sharper maximum of (001) parallel to the stretching direction (Fig. 4d–f). Similar weakening of CPO has been observed for, e.g., garnet and feldspars, where the deformation mechanism switched to diffusion accommodated grain-boundary sliding after grain

Table 1 Table showing the crystallographic relationships between plagioclase (Pl) and diopside (Di) for dominantly vermicular Cpx-Pl symplectites, the corresponding interplanar spacing (d) and the spacing ratio between plagioclase and diopside

Site	Angle range (°)	$(hkl)_{Pl}\|\|(hkl)_{Di}$	d_{Pl} (Å)	d_{Di} (Å)	d_{Pl}/d_{Di}
SZ-N-018-1	77–103	$(\bar{2}2\bar{3})\|\|(\bar{3}1\bar{2})$	1.531	1.700	0.90
		(223)||(312)	1.495	1.700	0.88
		(223)||(322)	1.495	1.612	0.93
		(131)||(121)	2.869	2.957	0.97
	140–170	$(01\bar{4})\|\|(\bar{1}0\bar{3})$	1.586	1.585	1.00
L-042-1	73–114	$(3\bar{1}\bar{1})\|\|(3\bar{1}\bar{1})$	2.657	2.895	0.92
L-042-2	135–160	$(1\bar{2}4)\|\|(3\bar{1}3)$	1.409	1.316	1.07

size reduction (e.g., Bestmann et al. 2008). Similarly, we infer that after the diopside grain size is reduced the Cpx-Pl symplectites deform by rigid-body rotation and grain boundary sliding accommodated by diffusion creep. This interpretation is further supported by our analysis of interphase misorientations, where the misorientation angle distribution of the most recrystallized and deformed symplectites show a tendency towards randomization (Fig. 7e–g), suggesting that the initially established crystallographic relationship is destroyed by rotation during grain boundary sliding.

Diffusion creep in anisotropic minerals coupled with rigid body rotation may lead to a CPO, where the crystallographic axis with the fastest reaction kinetics ends up parallel to the bulk stretching direction (Bons and den Brok 2000). Although much reduced in intensity with respect to the vermicular portions, the strong CPO of clinopyroxene observed in entirely recrystallized domains of the symplectites (Fig. 4d, f), with (001) parallel to the stretching lineation, is attributed to this process (e.g., Stünitz et al. 2020). Furthermore, the generally higher internal misorientation in the vermicular parts of symplectites, and the lack of significant misorientation in the granular parts, indicates that the grain size reduction coincides with a reduction of lattice distortion in diopside. The progressive grain size reduction of diopside will result in an increase of the phase boundary fraction and of the degree of phase mixing in the recrystallized symplectites (Kilian et al. 2011; Menegon et al. 2013; Ceccato et al. 2018). Increased phase mixing will inhibit grain growth due to second phase pinning, thereby further facilitating grain-size sensitive creep (e.g., Platt 2015; Ceccato et al. 2018).

Implications for fluid flow and crustal rheology

Cpx-Pl symplectites after omphacite are a common feature of nearly all eclogite occurrences worldwide (Wikström 1970a; Mysen 1972; Boland and van Roermund 1983; O'Brien 1989; Messiga and Bettini 1990; O'Brien et al. 1992; Möller 1998; Yang 2004; Anderson and Moecher 2007; Lanari et al. 2013; Martin and Duchêne 2015; Martin 2019; Feng et al. 2020; Dey et al. 2022; 2023; Schorn et al. 2023) and also have been investigated experimentally (Wikström 1970b). They have been suggested to assist eclogite exhumation (Dey et al. 2022), potentially even as a precursor for partial melting during the exhumation of ultra-high pressure rocks (Feng et al. 2020). Furthermore, Cpx-Pl symplectites represent the main breakdown reaction of omphacite and may thus significantly impact rheology and fluid-flow in eclogite-facies rocks during exhumation.

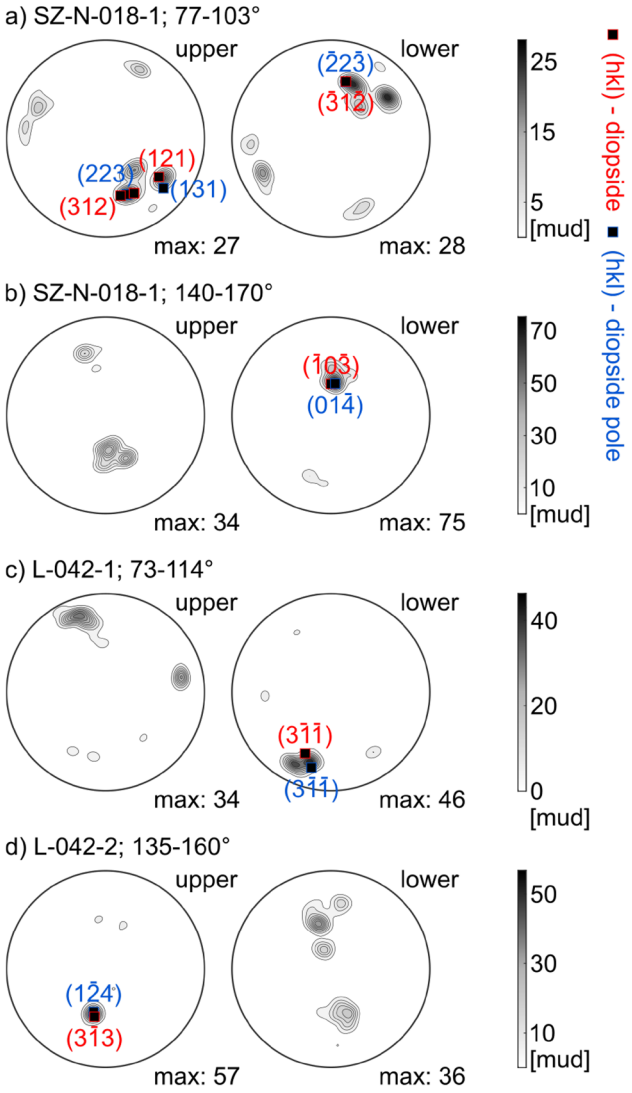

Fig. 8 Misorientation axis distributions of vermicular symplectites for specific angle ranges: **a** SZ-N-018-1 (vermicular); 77–103°; **b** SZ-N-018-1 (vermicular); 140–170°; **c** L-042-1 (vermicular); 73–114°; **d** L-042–2 (vermicular); 135–160°

As a decompression reaction, where the product has a lower density/larger volume, the symplectite forming reaction does not necessarily produce porosity (e.g., Okudaira et al. 2015). In our examples from sample WP039A (granular), the shear zone matrix surrounding the Cpx-Pl symplectites is composed of a fine-grained mixture of amphibole and plagioclase, while the Cpx-Pl symplectites contain only little amphibole. However, amphibole forms a rim around the Cpx-Pl symplectites (Figs. 3a, 4a). This microstructural relationship may indicate that if the interior of Cpx-Pl symplectites had the same abundance of aqueous fluid as the surrounding, the stable mineral assemblage would be amphibole + plagioclase, rather than diopside + plagioclase. This is supported by experimental results of Marti et al. (2017) on plagioclase-diopside mixtures, where nucleation of amphibole is observed particularly in high-strain zones. It follows that it is difficult for an aqueous fluid to infiltrate the Cpx-Pl symplectites. The reason for this is unknown. We speculate that the crystallographically well aligned interphase boundaries do not provide the necessary fluid pathways that random interphase boundaries would. The lack of porosity is also supported by the positive volume change from omphacite to symplectite. On the other hand, the inferred deformation by grain boundary sliding is expected to lead to creep cavitation processes, and thus create pathways for aqueous fluids to infiltrate the Cpx-Pl symplectites over time (e.g., Fusseis et al. 2009; Menegon et al. 2015).

In fact, the role of fluids during the symplectite forming reaction is somewhat enigmatic (see discussion in Anderson and Moecher 2007). Martin and Duchêne (2015) suggested that H_2O from hydrous minerals is necessary to destabilize omphacite, and thus for the reaction to occur. Similarly, O'Brien (1993) reports Cpx-Pl symplectites at omphacite grain boundaries, but not along quartz inclusions (in omphacite), indicating that a grain boundary fluid was necessary to trigger the reaction. However, as discussed above, significant amounts of aqueous fluid would likely lead to the formation of amphibole. In fact, Martin (2019) concluded that amphibole forms late by the hydration of diopside, i.e., not as part of the initial symplectite forming reaction. This is supported by the observation that the vermicular cores of the Cpx-Pl symplectites in WP039A (granular) generally do not contain amphibole. On the other hand, amphibole is abundant in the vermicular Cpx-Pl symplectite of SZ-N-018-1 (vermicular). The latter is the only sample from Holsnøy included in this study, where it has been shown that a significant amount of hydrous fluid was necessary to form the shear zone network, and that omphacite has high H_2O contents, up to 425 µg/g (Kaatz et al. 2021; 2022). Such data is not available from the Lofoten samples, but it seems plausible that the presence or absence of amphibole depends on the availability of H_2O during the reactions, and may be directly related to the H_2O content of the nominally anhydrous omphacite. With up to ~ 3000 ppm, omphacite has a higher maximum storage capacity for OH/H_2O than plagioclase (~ 1300 ppm) or diopside (~ 700 ppm; Katayama and Nakashima 2003; Johnson 2006; Skogby 2006). Therefore some H_2O must be released during the breakdown reaction. In line with previous studies, we speculate that some H_2O is necessary as a trigger for the breakdown reaction (e.g., O'Brien 1993; Martin and Duchêne 2015), but may be supplied internally in 'wet' eclogitic rocks.

The reaction studied here involves two changes that may impact bulk rheology: (i) the breakdown of omphacite to diopside and plagioclase, associated with grain size reduction, and (ii) the further grain size reduction of diopside during deformation of the Cpx-Pl symplectites. With regard to the former, the available data from deformation experiments on jadeite and diopside suggest that jadeite is stronger compared to diopside in the low-temperature plasticity regime (Dorner and Stöckhert 2004), but weaker in the dislocation creep regime (Orzol et al. 2006; Moghadam et al. 2010). In fact, intermediate compositions seem to be stronger than either endmember at high experimental temperatures (Moghadam et al. 2010). Experiments on diopside-plagioclase mixtures deforming by diffusion or dislocation creep have shown that such mixtures are much weaker deforming by diffusion creep, than the end-members are in the dislocation creep regime (Dimanov and Dresen 2005). It follows that the breakdown of omphacite leads to rock weakening, which is reinforced by the nucleation of plagioclase and how 'wet' the system is (Rybacki and Dresen 2000; Dimanov and Dresen 2005).

The grain size refinement of diopside during deformation of the Cpx-Pl symplectites is associated with a transition from brittle deformation to grain boundary sliding accommodated by diffusion creep. In that sense, brittle failure achieves the grain size reduction necessary to activate grain-size-sensitive creep. Deformation experiments on diopside-plagioclase mixtures suggest that (in the presence of fluid) deformation occurs by dissolution–precipitation creep of plagioclase and newly formed amphibole, while diopside is not intensely involved in the deformation (Marti et al. 2018). In a comparison between the deformation of orthopyroxene-plagioclase and amphibole-plagioclase mixtures, Mansard et al. (2020) found that amphibole-plagioclase mixtures are in general weaker, the magnitude of which depends on the starting material. In our deformed sample (WP039A; granular), the Cpx-Pl symplectites are surrounded by a matrix that dominantly consists of plagioclase and amphibole. The Cpx-Pl symplectites form variably stretched to sigmoidal aggregates wrapped by the shear zone matrix (Fig. 1d–f), suggesting that the Cpx-Pl symplectites are somewhat more rigid than the matrix, though the viscosity contrast is not necessarily very large. If our assessment of the limited permeability of Cpx-Pl symplectites and its increase during grain

boundary sliding are correct, it follows that with increasing deformation, progressively more amphibole would be present in the Cpx-Pl symplectite given sufficient availability of (internally or externally sourced) H_2O. Consequently, increasing deformation would be accompanied by reaction weakening as long as H_2O is available. From our considerations described above, the nucleation and deformation of Cpx-Pl symplectites thus leads to progressive rock weakening during the eclogite to amphibolite-facies transition.

Conclusions

We presented a detailed EBSD analysis of Cpx-Pl symplectites in a suite of retrogressed eclogites. From our analysis we draw the following conclusions.

1. Nucleation of Cpx-Pl symplectites replacing omphacite is achieved by topotaxial replacement of omphacite by diopside. The resulting expulsion of the jadeite-component of omphacite leads to the crystallographically controlled nucleation of plagioclase. The crystallographic relationship between plagioclase and diopside is such that lattice planes in the two minerals that are parallel have the same interplanar spacing.
2. Recrystallization and deformation of Cpx-Pl symplectites require grain size reduction of diopside, accommodated by fracturing. Deformation is then achieved by rigid-body rotation accommodated by grain-boundary sliding and diffusion creep, leading to weakening and a modification of the initially strong CPO of diopside and plagioclase. (001)-maxima of diopside parallel to the stretching direction result from crystallographically-controlled diffusion creep.
3. The formation of Cpx-Pl symplectites is not associated with an increase in permeability, and the deformation of said Cpx-Pl symplectites is necessary to enhance fluid flow in retrogressed eclogites. Furthermore, the successive deformation of Cpx-Pl symplectites and their hydration to form amphibole leads to progressive rock weakening.

Supplementary Information The online version contains supplementary material available at https://doi.org/10.1007/s00410-024-02125-0.

Acknowledgements This research was supported by the Deutsche Forschungsgemeinschaft (DFG, German Research Foundation) through grant 461241592 to SZ, and the Research Council of Norway through grant FRIPRO, no. 334965 to LM. The Research Council of Norway is acknowledged for support to the Goldschmidt Laboratory national infrastructure (project number 295894). Giorgio Pennacchioni is thanked for providing one of the samples. We thank Simon Schorn and an anonymous reviewer for constructive reviews that strengthened the paper and Dante Canil for editorial handling.

Author contributions SZ and LM designed the study. LFGM developed the methodology. Formal analysis and investigation were conducted by SZ. All authors discussed the results. SZ wrote the original draft and all authors contributed to review and editing. Funding acquisition by SZ and LM.

Funding Open access funding provided by University of Oslo (incl Oslo University Hospital).

Data availability The raw data is available at https://doi.org/10.5281/zenodo.10949549.

Declarations

Conflict of interest No conflicts of interest.

Consent to publication All listed authors consent to the publication of this article.

References

Anderson ED, Moecher DP (2007) Omphacite breakdown reactions and relation to eclogite exhumation rates. Contrib Miner Petrol 154:253–277. https://doi.org/10.1007/s00410-007-0192-x

Austrheim H (1987) Eclogitization of lower crustal granulites by fluid migration through shear zones. Earth Planet Sci Lett 81:221–232. https://doi.org/10.1016/0012-821X(87)90158-0

Austrheim H (1991) Eclogite formation and dynamics of crustal roots under continental collision zones. Terra Nova 3:492–499. https://doi.org/10.1111/j.1365-3121.1991.tb00184.x

Baïsset M, Labrousse L, Yamato P, Schubnel A (2023) Twinning and partial melting as early weakening processes in plagioclase at high pressure: insights from Holsnøy (Scandinavian Caledonides, Norway). Contrib Miner Petrol 178:19. https://doi.org/10.1007/s00410-023-01998-x

Bestmann M, Habler G, Heidelbach F, Thöni M (2008) Dynamic recrystallization of garnet and related diffusion processes. J Struct Geol 30:777–790. https://doi.org/10.1016/j.jsg.2008.02.007

Bhowany K, Hand M, Clark C, Kelsey DE, Reddy SM, Pearce MA, Tucker NM, Morrissey LJ (2018) Phase equilibria modelling constraints on P-T conditions during fluid catalysed conversion of granulite to eclogite in the Bergen Arcs, Norway. J Metamorph Geol 36:315–342. https://doi.org/10.1111/jmg.12294

Boland JN, van Roermund HLM (1983) Mechanisms of exsolution in omphacites from high temperature, type B, eclogites. Phys Chem Miner 9:30–37. https://doi.org/10.1007/BF00309467

Bons PD, den Brok B (2000) Crystallographic preferred orientation development by dissolution–precipitation creep. J Struct Geol 22:1713–1722. https://doi.org/10.1016/S0191-8141(00)00075-4

Bras E, Baïsset M, Yamato P, Labrousse L (2021) Transient weakening during the granulite to eclogite transformation within hydrous shear zones (Holsnøy, Norway). Tectonophysics 819:229026. https://doi.org/10.1016/j.tecto.2021.229026

Ceccato A, Menegon L, Pennacchioni G, Morales LFG (2018) Myrmekite and strain weakening in granitoid mylonites. Solid Earth 9:1399–1419. https://doi.org/10.5194/se-9-1399-2018

Centrella S (2019) The granulite- to eclogite- and amphibolite-facies transition: a volume and mass transfer study in the Lindås Nappe, Bergen Arcs, west Norway. Geol Soc Lond Spec Publ 478:241–264. https://doi.org/10.1144/SP478.9

Corfu F (2004) U-Pb age, setting and tectonic significance of the anorthosite–mangerite–charnockite–granite suite, Lofoten-Vesterålen, Norway. J Petrol 45:1799–1819. https://doi.org/10.1093/petrology/egh034

Crameri F (2018) Scientific colour-maps. Zenodo. https://doi.org/10.5281/zenodo.1243862

Deer WA, Howie RA, Zussman J (2013) An introduction to the rock-forming minerals. Mineral Socf Great Brit Ireland. https://doi.org/10.1180/dhz

Dewey JF, Ryan PD, Andersen TB (1993) Orogenic uplift and collapse, crustal thickness, fabrics and metamorphic phase changes: the role of eclogites. Geol Soc Lond Spec Publ 76:325–343. https://doi.org/10.1144/GSL.SP.1993.076.01.16

Dey A, Sen K, Mamtani MA (2022) Electron backscatter diffraction study of ultrahigh-pressure Tso Morari eclogites (Trans-Himalayan collisional zone): implications for strain regime transition from constrictional to plane strain during exhumation. Lithosphere 2022:7256746. https://doi.org/10.2113/2022/7256746

Dey A, Sen K, Sen A, Choudhary S (2023) Omphacite breakdown, symplectite formation and carbonate metasomatism in a retrograded continental eclogite: implications for the exhumation of the Tso Morari Crystalline Complex (Trans-Himalaya, NW India). Phys Chem Earth A/B/C 131:103453. https://doi.org/10.1016/j.pce.2023.103453

Dimanov A, Dresen G (2005) Rheology of synthetic anorthite-diopside aggregates: implications for ductile shear zones. J Geophys Res 110:B07203. https://doi.org/10.1029/2004JB003431

Dorner D, Stöckhert B (2004) Plastic flow strength of jadeite and diopside investigated by microindentation hardness tests. Tectonophysics 379:227–238. https://doi.org/10.1016/j.tecto.2003.11.008

Engi M, Giuntoli F, Lanari P, Burn M, Kunz B, Bouvier AS (2018) Pervasive eclogitization due to brittle deformation and rehydration of subducted basement: effects on continental recycling? Geochem Geophys Geosyst 19:865–881. https://doi.org/10.1002/2017GC007215

Eskola P (1921) On the eclogites of Norway. Videnskapsselskapets Skrifter I Mat Naturv Klasse I 8:1–118

Feng P, Wang L, Brown M, Johnson TE, Kylander-Clark A, Piccoli PM (2020) Partial melting of ultrahigh-pressure eclogite by omphacite-breakdown facilitates exhumation of deeply-subducted crust. Earth Planet Sci Lett 554:116664. https://doi.org/10.1016/j.epsl.2020.116664

Fournier HW, Lee JKW, Camacho A, Creaser RA (2014) Retrogression of eclogite-facies shear zones by short-lived fluid infiltration during the Caledonian orogeny, Lofoten islands, Norway. Geol Soc Lond Spec Publ 390:443–466. https://doi.org/10.1144/SP390.9

Froitzheim N, Miladinova I, Janák M, Kullerud K, Ravna EK, Majka J, Fonseca ROC, Münker C, Nagel TJ (2016) Devonian subduction and syncollisional exhumation of continental crust in Lofoten, Norway. Geology 44:223–226. https://doi.org/10.1130/g37545.1

Fusseis F, Regenauer-Lieb K, Liu J, Hough RM, De Carlo F (2009) Creep cavitation can establish a dynamic granular fluid pump in ductile shear zones. Nature 459:974–977. https://doi.org/10.1038/nature08051

Glodny J, Kühn A, Austrheim H (2008) Geochronology of fluid-induced eclogite and amphibolite facies metamorphic reactions in a subduction–collision system, Bergen Arcs, Norway. Contrib Miner Petrol 156:27–48. https://doi.org/10.1007/s00410-007-0272-y

Godard G (2001) Eclogites and their geodynamic interpretation: a history. J Geodyn 32:165–203. https://doi.org/10.1016/s0264-3707(01)00020-5

Heidelbach F, Terry MP (2013) Inherited fabric in an omphacite symplectite: reconstruction of plastic deformation under ultra-high pressure conditions. Microsc Microanal 19:942–949. https://doi.org/10.1017/s1431927613001451

Hielscher R, Schaeben H (2008) A novel pole figure inversion method: specification of the MTEX algorithm. J Appl Crystallogr 41:1024–1037. https://doi.org/10.1107/S0021889808030112

Jakob J, Andersen TB, Kjøll HJ (2019) A review and reinterpretation of the architecture of the South and South-Central Scandinavian Caledonides—a magma-poor to magma-rich transition and the significance of the reactivation of rift inherited structures. Earth Sci Rev 192:513–528. https://doi.org/10.1016/j.earscirev.2019.01.004

Jamtveit B, Bucher-Nurminen K, Austrheim H (1990) Fluid controlled eclogitization of granulites in deep crustal shear zones, Bergen arcs, Western Norway. Contrib Miner Petrol 104:184–193. https://doi.org/10.1007/bf00306442

Jamtveit B, Austrheim H, Malthe-Sorenssen A (2000) Accelerated hydration of the Earth's deep crust induced by stress perturbations. Nature 408:75–78. https://doi.org/10.1038/35040537

Jamtveit B, Dunkel KG, Petley-Ragan A, Austrheim H, Corfu F, Schmid DW (2021) Rapid fluid-driven transformation of lower continental crust associated with thrust-induced shear heating. Lithos 396:106216. https://doi.org/10.1016/j.lithos.2021.106216

Jaranowski M, Budzyń B, Barnes CJ, Majka J, Sláma J, Kozub-Budzyń GA, Kośmińska K (2023) U-Pb and trace element zircon and apatite petrochronology of eclogites from the Scandinavian Caledonides. Contrib Miner Petrol 178:47. https://doi.org/10.1007/s00410-023-02029-5

Joanny V, van Roermund H, Lardeaux JM (1991) The clinopyroxene/plagioclase symplectite in retrograde eclogites: a potential geothermobarometer. Geol Rundsch 80:303–320. https://doi.org/10.1007/BF01829368

Johnson EA (2006) Water in nominally anhydrous crustal minerals: speciation, concentration, and geologic significance. Rev Mineral Geochem 62:117–154. https://doi.org/10.2138/rmg.2006.62.6

Kaatz L, Zertani S, Moulas E, John T, Labrousse L, Schmalholz SM, Andersen TB (2021) Widening of hydrous shear zones during incipient eclogitization of metastable dry and rigid lower crust – Holsnøy, Western Norway. Tectonics 40:e2020TC006572. https://doi.org/10.1029/2020TC006572

Kaatz L, Reynes J, Hermann J, John T (2022) How fluid infiltrates dry crustal rocks during progressive eclogitization and shear zone formation: insights from H_2O contents in nominally anhydrous minerals. Contrib Miner Petrol 177:72. https://doi.org/10.1007/s00410-022-01938-1

Katayama I, Nakashima S (2003) Hydroxyl in clinopyroxene from the deep subducted crust: evidence for H_2O transport into the mantle. Am Miner 88:229–234. https://doi.org/10.2138/am-2003-0126

Kelly A (2012) Knowles KM Crystallography and crystal defects. Wiley, Chichester. https://doi.org/10.1002/9781119961468

Kilian R, Heilbronner R, Stünitz H (2011) Quartz grain size reduction in a granitoid rock and the transition from dislocation to

diffusion creep. J Struct Geol 33:1265–1284. https://doi.org/10.1016/j.jsg.2011.05.004
Labrousse L, Jolivet L, Andersen TB, Agard P, Hébert R, Maluski H, Schärer U, Whitney DL, Teyssier C, Siddoway CS (2004) Pressure-temperature-time deformation history of the exhumation of ultra-high pressure rocks in the Western Gneiss Region, Norway. In: Whitney DL, Teyssier C, Siddoway CS (eds) Gneiss domes in orogeny. Geological Society of America, Boulder, pp 155–183. https://doi.org/10.1130/0-8137-2380-9.155
Lanari P, Riel N, Guillot S, Vidal O, Schwartz A, Pêcher A, Hattori KH (2013) Deciphering high-pressure metamorphism in collisional context using microprobe mapping methods: application to the Stak eclogitic massif (northwest Himalaya). Geology 41:111–114. https://doi.org/10.1130/g33523.1
Li X, Zhang L, Wei C, Slabunov AI, Bader T (2018) Quartz and orthopyroxene exsolution lamellae in clinopyroxene and the metamorphic P-T path of Belomorian eclogites. J Metamorph Geol 36:1–22. https://doi.org/10.1111/jmg.12280
Lloyd GE, Farmer AB, Mainprice D (1997) Misorientation analysis and the formation and orientation of subgrain and grain boundaries. Tectonophysics 279:55–78. https://doi.org/10.1016/S0040-1951(97)00115-7
Mansard N, Stünitz H, Raimbourg H, Précigout J, Plunder A, Nègre L (2020) Relationship between microstructures and resistance in mafic assemblages that deform and transform. Solid Earth 11:2141–2167. https://doi.org/10.5194/se-11-2141-2020
Markl G, Bucher K (1997) Proterozoic eclogites from the Lofoten islands, northern Norway. Lithos 42:15–35. https://doi.org/10.1016/S0024-4937(97)00034-0
Markl G, Frost BR, Bucher K (1998) The origin of anorthosites and related rocks from the Lofoten Islands, Northern Norway: I. Field relations and estimation of intrinsic variables. J Petrol 39:1425–1452. https://doi.org/10.1093/petroj/39.8.1425
Marti S, Stünitz H, Heilbronner R, Plümper O, Drury M (2017) Experimental investigation of the brittle-viscous transition in mafic rocks—interplay between fracturing, reaction, and viscous deformation. J Struct Geol 105:62–79. https://doi.org/10.1016/j.jsg.2017.10.011
Marti S, Stünitz H, Heilbronner R, Plümper O, Kilian R (2018) Syn-kinematic hydration reactions, grain size reduction, and dissolution–precipitation creep in experimentally deformed plagioclase–pyroxene mixtures. Solid Earth 9:985–1009. https://doi.org/10.5194/se-9-985-2018
Martin C (2019) P-T conditions of symplectite formation in the eclogites from the Western Gneiss Region (Norway). Geol Soc Lond Spec Publ 478:197–216. https://doi.org/10.1144/SP478.18
Martin C, Duchêne S (2015) Residual water in hydrous minerals as a kinetic factor for omphacite destabilization into symplectite in the eclogites of Vårdalsneset (WGR, Norway). Lithos 232:162–173. https://doi.org/10.1016/j.lithos.2015.06.021
McNamara DD, Wheeler J, Pearce M, Prior DJ (2012) Fabrics produced mimetically during static metamorphism in retrogressed eclogites from the Zermatt-Saas zone, Western Italian Alps. J Struct Geol 44:167–178. https://doi.org/10.1016/j.jsg.2012.08.006
Menegon L, Stünitz H, Nasipuri P, Heilbronner R, Svahnberg H (2013) Transition from fracturing to viscous flow in granulite facies perthitic feldspar (Lofoten, Norway). J Struct Geol 48:95–112. https://doi.org/10.1016/j.jsg.2012.12.004
Menegon L, Fusseis F, Stünitz H, Xiao X (2015) Creep cavitation bands control porosity and fluid flow in lower crustal shear zones. Geology 43:227–230. https://doi.org/10.1130/G36307.1
Messiga B, Bettini E (1990) Reactions behaviour during kelyphyte and symplectite deformation: a case study of mafic granulites and eclogites from the Bohemian Massif. Eur J Mineral 2:125–144
Moghadam RH, Trepmann CA, Stöckhert B, Renner J (2010) Rheology of synthetic omphacite aggregates at high pressure and high temperature. J Petrol 51:921–945. https://doi.org/10.1093/petrology/egq006
Möller C (1998) Decompressed eclogites in the Sveconorwegian (–Grenvillian) orogen of SW Sweden: petrology and tectonic implications. J Metamorph Geol 16:641–656. https://doi.org/10.1111/j.1525-1314.1998.00160.x
Moore J, Beinlich A, Porter JK, Talavera C, Berndt J, Piazolo S, Austrheim H, Putnis A (2020) Microstructurally controlled trace element (Zr, U-Pb) concentrations in metamorphic rutile: an example from the amphibolites of the Bergen Arcs. J Metamorph Geol 38:103–127. https://doi.org/10.1111/jmg.12514
Morales LFG (2022) Interphase misorientation as a tool to study metamorphic reactions and crystallization in geological materials. Am Miner 107:1501–1518. https://doi.org/10.2138/am-2021-7902
Morales LFG, Mainprice D, Kern H (2018) Olivine-antigorite orientation relationships: Microstructures, phase boundary misorientations and the effect of cracks in the seismic properties of serpentinites. Tectonophysics 724–725:93–115. https://doi.org/10.1016/j.tecto.2017.12.009
Mysen BO (1972) Five clinopyroxenes in the Hareidland eclogite, Western Norway. Contrib Miner Petrol 34:315–325. https://doi.org/10.1007/BF00373761
Mysen B, Griffin WL (1973) Pyroxene stoichiometry and the breakdown of omphacite. Am Miner 58:60–63
Neumann B (2000) Texture development of recrystallised quartz polycrystals unravelled by orientation and misorientation characteristics. J Struct Geol 22:1695–1711. https://doi.org/10.1016/S0191-8141(00)00060-2
O'Brien PJ (1989) A study of retrogression in eclogites of the Oberpfalz Forest, north-east Bavaria, West Germany, and their significance in the tectonic evolution of the Bohemian Massif. Geol Soc Lond Spec Publ 43:507–512. https://doi.org/10.1144/GSL.SP.1989.043.01.48
O'Brien PJ (1993) Partially retrograded eclogites of the Münchberg Massif, Germany: records of a multi-stage Variscan uplift history in the Bohemian Massif. J Metamorph Geol 11:241–260. https://doi.org/10.1111/j.1525-1314.1993.tb00145.x
O'Brien PJ, Röhr C, Okrusch M, Patzak M (1992) Eclogite facies relics and a multistage breakdown in metabasites of the KTB pilot hole, NE Bavaria: implications for the Variscan tectonometamorphic evolution of the NW Bohemian Massif. Contrib Miner Petrol 112:261–278. https://doi.org/10.1007/BF00310460
Okudaira T, Jeřábek P, Stünitz H, Fusseis F (2015) High-temperature fracturing and subsequent grain-size-sensitive creep in lower crustal gabbros: evidence for coseismic loading followed by creep during decaying stress in the lower crust? J Geophys Res Solid Earth 120:3119–3141. https://doi.org/10.1002/2014JB011708
Orzol J, Stöckhert B, Trepmann CA, Rummel F (2006) Experimental deformation of synthetic wet jadeite aggregates. J Geophys Res 111:B06205. https://doi.org/10.1029/2005JB003706
Platt JP (2015) Rheology of two-phase systems: a microphysical and observational approach. J Struct Geol 77:213–227. https://doi.org/10.1016/j.jsg.2015.05.003
Putnis A, Moore J, Prent AM, Beinlich A, Austrheim H (2021) Preservation of granulite in a partially eclogitized terrane: metastable phenomena or local pressure variations? Lithos 400–401:106413. https://doi.org/10.1016/j.lithos.2021.106413
Raimbourg H, Jolivet L, Labrousse L, Leroy Y, Avigad D (2005) Kinematics of syneclogite deformation in the Bergen Arcs, Norway: implications for exhumation mechanisms. Geol Soc Lond Spec Publ 243:175–192. https://doi.org/10.1144/gsl.sp.2005.243.01.13
Raimbourg H, Jolivet L, Leroy Y (2007) Consequences of progressive eclogitization on crustal exhumation, a mechanical study.

Geophys J Int 168:379–401. https://doi.org/10.1111/j.1365-246X.2006.03130.x

Rybacki E, Dresen G (2000) Dislocation and diffusion creep of synthetic anorthite aggregates. J Geophys Res Solid Earth 105:26017–26036. https://doi.org/10.1029/2000JB900223

Schorn S, Rogowitz A, Hauzenberger CA (2023) Partial melting of amphibole–clinozoisite eclogite at the pressure maximum (eclogite type locality, Eastern Alps, Austria). Eur J Mineral 35:715–735. https://doi.org/10.5194/ejm-35-715-2023

Skogby H (2006) Water in natural mantle minerals I: pyroxenes. Rev Mineral Geochem 62:155–167. https://doi.org/10.2138/rmg.2006.62.7

Smyth JR (1980) Cation vacancies and the crystal chemistry of breakdown reactions in kimberlitic omphacites. Am Miner 65:1185–1191

Spruzeniece L, Piazolo S, Maynard-Casely HE (2017) Deformation-resembling microstructure created by fluid-mediated dissolution–precipitation reactions. Nat Commun 8:14032. https://doi.org/10.1038/ncomms14032

Steltenpohl M, Hames W, Andresen A, Markl G (2003) New Caledonian eclogite province in Norway and potential Laurentian (Taconic) and Baltic links. Geology 31:985–988. https://doi.org/10.1130/G19744.1

Steltenpohl MG, Kassos G, Andresen A, Rehnström EF, Hames WE (2011) Eclogitization and exhumation of Caledonian continental basement in Lofoten, North Norway. Geosphere 7:202–218. https://doi.org/10.1130/GES00573.1

Stünitz H, Neufeld K, Heilbronner R, Finstad AK, Konopásek J, Mackenzie JR (2020) Transformation weakening: diffusion creep in eclogites as a result of interaction of mineral reactions and deformation. J Struct Geol 139:104129. https://doi.org/10.1016/j.jsg.2020.104129

Wheeler J, Prior D, Jiang Z, Spiess R, Trimby P (2001) The petrological significance of misorientations between grains. Contrib Miner Petrol 141:109–124. https://doi.org/10.1007/s004100000225

Wikström A (1970a) Electron microprobe studies of the alteration of omphacite in eclogites from the Nordfjord area, Norway. Nor Geol Tidsskr 50:135–155

Wikström A (1970b) Hydrothermal experiments in the system jadeite-diopside. Nor Geol Tidsskr 50:1–14

Yang TN (2004) Retrograded textures and associated mass transfer: evidence for aqueous fluid action during exhumation of the Qinglongshan eclogite, Southern Sulu ultrahigh pressure metamorphic terrane, eastern China. J Metamorph Geol 22:653–669. https://doi.org/10.1111/j.1525-1314.2004.00540.x

Zertani S, Labrousse L, John T, Andersen TB, Tilmann F (2019) The interplay of eclogitization and deformation during deep burial of the lower continental crust—a case study from the Bergen Arcs (western Norway). Tectonics 38:898–915. https://doi.org/10.1029/2018tc005297

Zertani S, John T, Brachmann C, Vrijmoed JC, Plümper O (2022) Reactive fluid flow guided by grain-scale equilibrium reactions during eclogitization of dry crustal rocks. Contrib Miner Petrol 177:61. https://doi.org/10.1007/s00410-022-01928-3

Zertani S, Menegon L, Pennacchioni G, Buisman I, Corfu F, Jamtveit B (2023) Protracted localization of metamorphism and deformation in a heterogeneous lower-crustal shear zone. J Struct Geol 176:104960. https://doi.org/10.1016/j.jsg.2023.104960

Zhong X, Andersen NH, Dabrowski M, Jamtveit B (2019) Zircon and quartz inclusions in garnet used for complementary Raman thermobarometry: application to the Holsnøy eclogite, Bergen Arcs, Western Norway. Contrib Miner Petrol 174:50. https://doi.org/10.1007/s00410-019-1584-4